Optimization Design of Hull Compartment Structure based on 3D Modeling

Jing Wu, Yaqi Liu*
School of Naval Architecture and Ocean Engineering, Jiangsu Shipping College Nantong, 226010, China
E-mail: 13405740807@163.com, 15950881644@163.com
*Corresponding author

Keywords: 3D modeling; Cabin section; Oil tankers; Components; BP neural network; PSO algorithm

Received: June 19, 2024

The study constructs a three-dimensional model by using finite element software to optimize the hull compartment structure. The optimized design variables are obtained through sensitivity analysis. At the same time, the study uses particle swarm optimization algorithm to improve the back-propagation neural network. The improved algorithm is optimized by using the staged mutation strategy and chaotic search to realize the optimization calculation of the hull compartment structure. Real sample data are obtained through orthogonal tests and relevant validation is carried out. The experimental validation showed that the minimum optimal equivalent stress solution of the proposed method was 0.167, which was 1.7041 less than the back propagation neural network algorithm based on particle swarm optimization. The maximum optimal shear stress solution of the proposed method was 0.0640, which was 0.9761 less than the comparison algorithm. The equivalent stresses of the inner sole plate before and after optimization were 140N/mm^2 and 160N/mm^2, respectively. Compared with the other methods, the accuracy of the proposed method was increased by 19.31%, 3.75%, and 2.96% over the three compared methods, respectively. As a result, the algorithmic computational efficiency and the ability to find the optimum can be improved by combining the staged mutation strategy with the particle swarm optimization algorithm to improve the back propagation neural network. The proposed method can effectively improve the stress of the cockpit components and realize the structural optimization. This method has positive application significance in the optimal design of ship cabin structure.

Povzetek: V članku je opisan tridimenzionalni model za optimizacijo strukture ladijskih predelov s pomočjo metode končnih elementov. Uporaba izboljšanega nevronskega omrežja s strategijo mutacije in kaotičnim iskanjem izboljšuje strižne napetosti in stresne točke, kar prispeva k večji stabilnosti in optimizaciji ladijske strukture.

1 Introduction

As an important water transportation vehicle, the design of the hull structure of oil tankers directly affects the safety, economy, and environmental friendliness of the vessel [1-3]. In the design of oil tankers, the optimization of the hull compartment is important to improve the performance. The layouts, dimensions, and weight distributions of the cabin structure should be accurately calculated and comprehensively considered to ensure the stability and durability of the vessel during transportation [4-6]. Many researchers begin to explore the application of artificial intelligence algorithms in the optimization of hull structures to further improve the accuracy and efficiency of design [7]. Among these artificial intelligence algorithms, the Back Propagation (BP) neural network is a commonly used machine learning method. BP neural network shows better advantages in dealing with complex problems by simulating the learning mechanism of humans. The basic idea of BP is to modify the weights and thresholds of the network. This can be achieved through the mean square error between the actual output of the neural network and the desired output of the sample. Then the actual output mean square error of the network reaches the target value. BP has been widely used in the optimal design of hull structure such as total hull resistance and uniformity of companion flow on the pulp disc surface. The BP neural network is effective in many fields. However, there are still some limitations in the practical application, such as the problem of easily falling into local optima [8]. Therefore, it is necessary to improve the BP neural network. Particle Swarm Optimization (PSO) has the advantages of simple structure, few parameters, and easy to implement. Its improvement strategy for combining with other algorithms has been studied more. In view of this, this study focused on the structure of oil tanker compartments, conducted finite element analysis, and introduced the BP neural network. Meanwhile, the improvement methods and applications in optimization compartment structures were explored to effectively optimize the structure of ship compartments. The goal of the optimization is to develop

an optimized design method for the structure of ship compartments. In this way, the automation and intelligence of the structural design of oil tanker compartments can be achieved. Then the performance indicators of the hull can be more accurately predicted and the structure of the hull can be optimized. The artificial intelligence algorithms in the structural design of oil tanker compartments are introduced for structural optimization. This is beneficial for improving the intelligence of structural design and providing important references for ship structural design. The study is divided into four parts. The first part is a literature review, which introduces the research status of the ships and the BP neural network. The second part is to conduct finite element analysis and sensitivity analysis of the oil tanker compartment structure. Meanwhile, sample data are obtained, and relevant predictions are carried out through the improved BP neural network. In the third part, the results are analyzed, the effectiveness of improving the BP neural network and optimizing the structure is studied, and a discussion section is added. In the fourth part, the research methods are summarized, and the research shortcomings and future research directions are pointed out.

2 Related Works

The early oil tanker was a single-shell structure, which had structural stability defects. The hull may be damaged. The crude oil may leak when collisions occur, resulting in negative impacts on the marine ecology. Therefore, it is necessary to optimize the design of the hull. Lian F et al. considered the various costs of shipping companies to improve the overall efficiency. Meanwhile, a method was proposed to determine the optimal vessel and weekly service frequency to minimize total costs. The results showed that the optimal size was smaller than the currently largest in-service container ship [9]. Dai R et al. made improvements in the topology optimization and other aspects of solid plates for pressure resistant hull outer compartments to simplify the construction and reduce the weight of the solid plate. The strength of the entire structure was analyzed using Hyperworks/Optimization. The results showed that the maximum stress of the solid plate after topology optimization was the smallest. The weight of the solid plate after optimizing the diameter of aperture was reduced by 19%. The shear stress was increased by 38% [10]. Ameen N M et al. proposed a new method for robust nonlinear Proportional-Integral-Derivative (PID) controllers to improve the response speed of the system and reduce the impact of nonlinearity and uncertainty. Nonlinear functions were added. Differential terms in conventional PID controllers were filtered. Then the corresponding controller gain was adjusted. The results indicated that the system had good performance, with good performance in zero steady-state error and better transient response [11]. Guo S et al. designed an autonomous path planning method based on deep reinforcement learning to improve the automation of unmanned ships' path planning in unknown environments. The method combined deep deterministic strategy gradient algorithm and simulated the optimal action strategy based on relevant empirical data. The navigation restriction areas were set to improve the effectiveness of the method. The experimental results showed that the proposed method had a good convergence speed and ran stably [12]. Zakerdoost H et al. proposed a framework to optimize the performance of ship propeller systems in waves. This framework determined the main geometric characteristics and optimized them under two levels and multi-point operating conditions. Methods such as multi-objective evolutionary algorithms were adopted to minimize the effective power and maximize the propulsion efficiency. A semi-empirical formula was used to estimate the additional wave resistance. The results indicated that the proposed method was effective [13].

Zhang Z et al. introduced the BP neural network to predict the ship traffic flow in the designated port area. The parameters of the BP neural network were optimized by improving the PSO algorithm. The analysis of the ship traffic flow was conducted through the obtained model. The test results showed that the method had good predictive performance and good convergence [14]. Liu Y et al. proposed a method based on the empirical mode decomposition, genetic algorithm, and BP neural network to more accurately evaluate the state of rolling bearings. First, the vibration signals were decomposed, features were extracted, and then the parameters of the BP neural network were optimized. The proposed method had a high accuracy after verification with relevant bearing datasets [15]. Lu J et al. proposed a boiler steam pressure control system based on the BP-PID control to improve the boiler steam pressure control and address the shortcomings of traditional PID control methods. The simulation results showed that the PID controller based on the BP neural network achieved better control performance, with no oscillation, no overshoot, and short transition time in the response curve [16]. Zhang D proposed a diagnostic method based on the adaptive neural network to improve the accuracy and timeliness of ship power plant fault diagnosis. This method was applied to fault detection and estimation, effectively solving the limited applicability and low accuracy of current ship equipment fault identification methods. The simulation results showed that the model effectively reduced fault diagnosis errors and diagnosed faults faster and more effectively [17]. When Pany C et al. studied the axis of an infinitely long cylindrical curved plate. They conducted relevant research based on finite element combined with wave methods to understand the bending vibration natural frequency. The results showed that the proposed method effectively reduced computational complexity and had a good application effect [18]. Pany C et al. introduced the finite element method and

conducted relevant analysis to understand the propagation of free waves in two-dimensional periodic plates. From the obtained results, the proposed method effectively described the propagation of free waves [19]. Pany C et al. introduced triangular finite element method to investigate the flutter of periodic supported curved plates. This method achieved high accuracy and was used for flutter analysis. The results showed that the proposed method had good accuracy [20].

In summary, with the complexity of hull, there are characteristics such as high dimensionality and high nonlinearity in the optimization problems of the ship research. Traditional methods are difficult to deal with these problems. However, BP neural network is a good artificial neural network with strong adaptability and self-learning ability, which has significant advantages in high non-linear problems. The relationship between ship geometric parameters and structural response is highly nonlinear, making it very suitable for predicting structural response output. Therefore, the study applies the BP neural network to optimize the hull section of oil tankers. To solve the local minimum, this study aims to improve the algorithm to achieve structural optimization of oil tankers. The study introduces the BP neural network to intelligently optimize the cabin structure of oil tankers, which has certain reference value for optimizing the structural design. The unstable generalization ability of the BP neural network can be optimized by adopting a new PSO algorithm, which may improve the BP neural network to handle high nonlinearity problems. In addition, the study further compares the differences between the existing methods and the proposed method to effectively illustrate the need for the study, as shown in Table 1.

Table 1: Comparison of the proposed method with existing methods

References	Methods	Results	limitations
Lian F et al. [9]	Determine the optimum ship size and number of services per week to minimise the total cost, taking into account the costs to shipping companies in various areas	Optimum size should be smaller than the largest container ship currently in service	Theoretical optimization of hull structure dimensions from an economic point of view only
Dai R et al. [10]	Strength characterization of the entire structure using Hyperworks/Optimization	Topology optimizes solid plate with the minimum-maximum stress value	Require hundreds or thousands of iterations and is time consuming
Ameen N M et al. [11]	Add a nonlinear function to a conventional PID controller and filter the differential term, and tuning the corresponding controller gain	The performance of the system is better in terms of zero steady state error with better transient response	High computational effort, poor convergence performance, and difficult to obtain effective gradient information
Guo S et al. [12]	An autonomous path planning approach combining deep deterministic policy gradient algorithms	Better convergence speed, able to run stably	Higher computational volume
Zakerdoost H et al. [13]	Methods such as multi-objective evolutionary algorithms are used to minimize the effective power and maximize the propulsive efficiency. Semi-empirical formulas are used to estimate the additional wave resistance.	Optimize the performance of a hull propeller system in waves	The method relies on training data and is not efficient enough for structural optimization of the agent model
This paper	Analyze the structure of ship's cabin segments by Three-Dimensional (3D) modeling based on finite element analysis and construct an optimization model with the BP improved by PSO	Reduce computation, improve iterative efficiency, and effectively enhance the stresses in compartment members for structural optimization	-

3 Optimization design of oil tanker structure on the ground of 3D modeling and improved BP neural network

Firstly, finite element analysis of the tanker compartment is carried out. A 3D two-compartment model is constructed to optimize the tanker compartment structure. Secondly, the stress results of the hull components under the most hazardous working conditions are analyzed to determine whether the tanker internal structure could be

optimized. Sensitivity analysis and sample collection of the compartment structure are then performed. The PSO algorithm is optimized by using a staged mutation strategy. The MIPSO-BP and SMPSO-BP neural networks are proposed.

3.1 Finite element analysis, sensitivity analysis, and sample acquisition of hull compartment structure

Hull structural analysis is an important part of ship design. With the continuous advancement of technology and the increasing complexity of hull structures, traditional regulatory methods are able to meet the needs of modern ship design. The finite element analysis gradually becomes a main method for hull structural analysis. This method can more accurately simulate the actual stress and deformation of hull. First, the cabin is analyzed using finite element software to understand the sensitivity of the model. Meanwhile, the BP neural network is trained, and samples are obtained. Subsequently, the PSO algorithm is improved through a staged mutation strategy. Meanwhile, the improved algorithm is used to optimize the BP neural network. The design of oil tanker structure optimization is achieved by improving the BP neural network after constructing a mathematical model for optimizing the cabin structure. The performance of the BP neural network is improved by optimizing the PSO algorithm. A mathematical model for optimizing the cabin structure is constructed. The constructed optimization mathematical model can provide an important theoretical basis for the optimization of hull structures. In this regard, a finite element analysis is conducted on the cabin section of the 107600DWT RAMAX oil tanker to understand whether there is room for structural optimization. ANSYS software is chosen for finite element analysis. Overall, the structure of the study is shown in Figure 1.

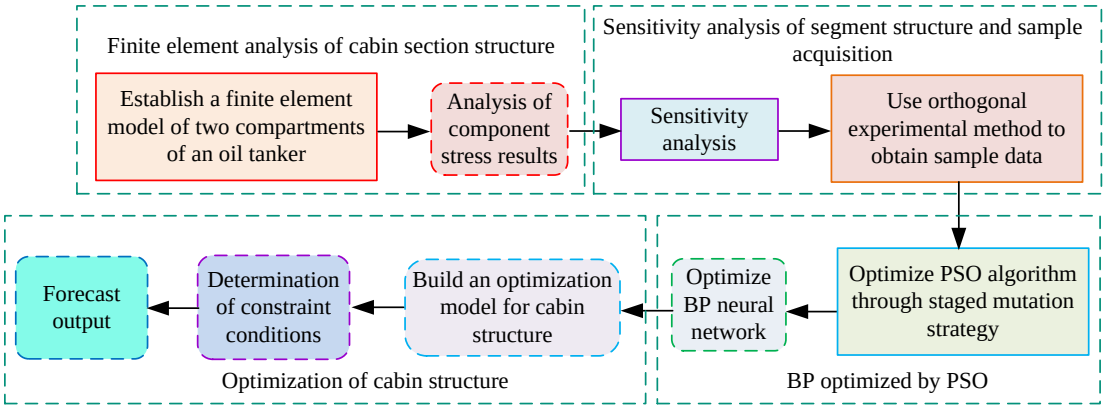

Figure 1: Research structure

In Figure 1, this structure includes sections such as cabin model construction and sample acquisition. Firstly, the cabin segment model is constructed using finite element software. Among them, the ship adopts a double shell longitudinal skeleton structure, with 6 cargo oil tanks. The relevant parameters of the ship are shown in Table 2.

Table 2: Relevant parameters

Parameter	Total length (m)	Length between vertical lines (m)	Standard captain (m)	Shape width (m)	Shape depth (m)	Structure draft (m)
Value	243.80	237.00	237.00	42.00	21.30	14.55
Parameter	Ballast draft (m)	Square coefficient	Structure draft displacement (t)	Rib spacing (FR.49-FR.79) (meters)	Rib spacing (FR.79-FR.86) (meters)	
Value	8.50	0.8557	127037	4.93	4.58	

In Table 2, the oil tank area is Frame (FR) 49-FR.86, with a total length of 243.80m and a ballast draft of 8.50m. The entire ship model is replaced with a segment model. Meanwhile, the overall coordinate system of the finite element model of the segment structure is established by using a right-handed Cartesian coordinate system. The coordinate origin of this model is at the intersection of rib 61 on the longitudinal section of the

ship and the baseline. The X-axis, Y-axis, and Z-axis are set. In the cabin model, two cabin models are selected. Meanwhile, the structural limit evaluation object is a complete cargo oil tank in the middle of the ship. The boundary is the front and rear hull structure of the cargo oil tank. The relevant structure of the cabin section is shown in Figure 2.

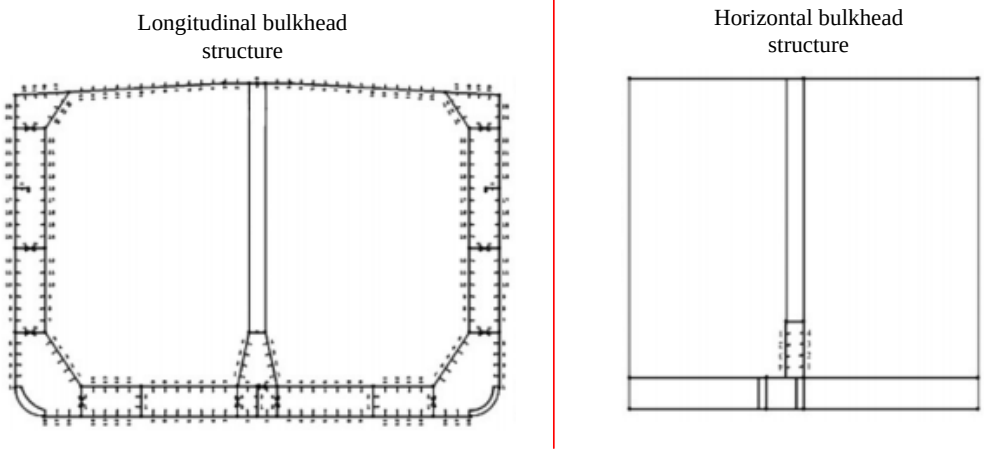

Figure 2: The relevant structure of the cabin section

Figure 2 shows the structure of longitudinal and transverse bulkheads. Half of the complete oil tank can be taken forward and backward to weaken the influence of boundary conditions on structural response. Then a 1/2+1+1/2 tank segment calculation model is formed. In this regard, the entire No.3 oil tank and 1/2 of the No.2 and No.4 oil tanks are taken for finite element modeling. During the grid division, attention should be paid to the type, number, and shape of the grid. Fewer triangular elements should be used. In general, the finite element mesh of the cabin structure is divided longitudinally based on rib spacing or similar spacing and horizontally based on longitudinal spacing or similar spacing, with the mesh shape as close to a square as possible. Meanwhile, the aspect ratio of plate elements is usually less than 3. Triangular elements should be avoided in areas of high stress or high stress gradient. The aspect ratio of plate elements should be close to 1. There are two types of material property settings, namely SAH and AH steel materials. These two materials yield stresses are 355MPa and 315MPa, respectively. These two materials have ultimate tensile strength of 726MPa and 513MPa, corresponding elongation of 16% and 22%, respectively. The stress-strain curves of the two materials are shown in Figure 3.

In Figure 3, the stress-strain curve of the two materials is located above the SAH steel material. As the strain increases, the curves show a trend of first increasing and then decreasing. Specific material parameters are shown in Table 3.

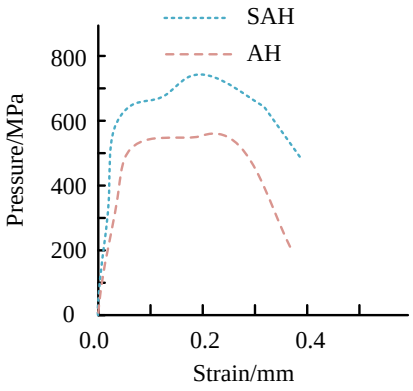

Figure 3: Stress-strain curve

Table 3: Main parameters of materials

Parametric	Parameter value
AH material factor for high strength steel	0.78
SAH material factor for high strength steel	0.72
Modulus of elasticity	$2.06\times1011N/m^2$
Poisson's ratio	0.3
Bulk density	7850 kg/m3
Gravitational acceleration	9.81 m/s2

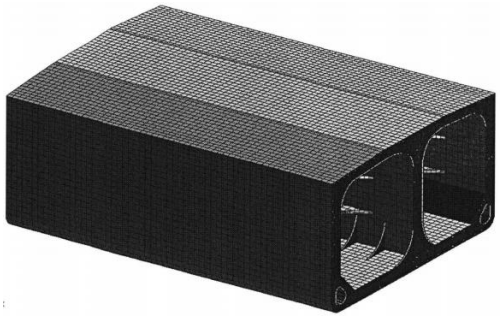

Figure 4: The relevant structure of the cabin section

According to the parameters set in Table 3, a 3D two-compartment segment model is constructed with 24637 nodes and 44900 cells. The finite element model of the cabin section is shown in Figure 4.

From Figure 4, the constructed 3D two-compartment model is in good condition. The deck, side outer plate, ship bottom plate, longitudinal and transverse bulkheads, rib plates, and other plates of the cabin section are simulated using four-node or three-node plate elements. Meanwhile, longitudinal bones, reinforcing ribs, and other bone materials are simulated using two-node beam elements. At the same time, the actual cross-section and eccentricity of each bone component are taken into account. During the model construction, each node has 6 degrees of freedom, namely 3 translational degrees of freedom (displacement in the x, y, and z axes) and 3 rotational degrees of freedom (rotation around the x, y, and z axes). These degrees of freedom may vary depending on the type of element established. For example, beam elements typically have 1 to 2 rotational degrees of freedom. The selected oil tanker type for research is relatively large, which mainly bears four types of loads, namely hull water pressure, cargo load, ship weight, and cabin end bending moment. Among them, the outboard water pressure includes two situations, namely full and non-full load draft conditions. The water pressure outside the hull is composed of static water pressure and wave hydrodynamic pressure under full load conditions. The relevant expression of the reference water pressure is shown in equation (1).

$$\begin{cases} P_0 = C_w - 0.67(D-d) \\ C_w = \begin{cases} 10.75 - \left(\dfrac{300-L}{100}\right)^{3/2} & 90 \le L \le 300 \\ 10.75 & 300 \le L \le 350 \\ 10.75 - \left(\dfrac{L-350}{150}\right)^{3/2} & 350 \le L \end{cases} \end{cases} \quad (1)$$

In equation (1), P_0 represents the reference water pressure, the unit of P_0 is kN/m2. C_w represents the wave coefficient. The mold depth is set to D. L represents the standard ship length. d represents the draft of the design structure. The units of D, L, and d are all in meters. The calculation formula for the pressure of liquid cargo in the cabin is shown in equation (2).

$$P = \rho_0 g(h + 2.5) \quad (2)$$

In equation (2), P represents the pressure of liquid cargo in the tank, which is measured in kN/m2. The density of liquid cargo in the tank is set to ρ_0, and the unit is t/m3. The gravitational acceleration is set to g, with a value of 9.81m/s2. The vertical distance from the top of the cabin to the calculation point is set to h, with a unit of m. Considering the pressure of steam and other factors inside the cabin, an additional head of 2.5m is set. The self-weight of the ship is the weight of the empty ship in the cabin section. In the finite element analysis, mass density and gravitational acceleration are set and applied to the model. In addition, it is necessary to calculate the end face bending moment as the boundary condition for the forces on the two end faces, and the relevant calculation formula is shown in equation (3).

$$M = M_s + M_w - M_r \quad (3)$$

In equation (3), M is the end face bending moment. The wave bending moment is set to M_w. The static water bending moment is set to M_s. The corrected bending moment is set to M_r. When there is no M_s under the corresponding working condition, there is M_r. It is unable to determine the maximum static water bending moment M_s under the corresponding working condition. Therefore, it is necessary to correct the static water bending moment according to the guidelines. M_r is an additional bending moment caused by local loads. Among them, the relevant expression of M_r is shown in equation (4).

$$M_r = \frac{3}{32} Q_m L_0^2 + \frac{1}{32} Q_e L_0^2 \quad (4)$$

In equation (4), L_0 represents the total length of the cabin model, which is measured in meters, and M_r is measured in kN*m. The linear uniformly distributed pressure of the middle compartment model is set Q_m. The linear uniformly distributed pressure of the two end compartments is set Q_e. The units of Q_m and Q_e are the same, both in kN/m. The boundary conditions applied at both ends of the cabin include force and displacement boundary conditions when applying the cabin model for finite element analysis. The boundary condition of force, namely the end face bending moment, represents the constraints on the cabin section at both ends. The displacement boundary condition restricts the rigid body displacement (linear displacement and angular displacement) of the model. If the boundary conditions are not constrained, the singularity in the structural stiffness matrix of finite element analysis may occur, resulting in solution failure or incorrect stress results. There are many nodes at both ends of the cabin model. It would be more laborious and time-consuming to impose the constraints one by one. Boundary conditions are applied through multi-point constraint forms. The specific boundary conditions are shown in Table 4.

In Table 4, Cons represents a fixed displacement of 0 in that direction. Link represents the displacement of

relevant points within the end face connected to independent points. BM indicates the application of end face bending moment in this direction. δ_x, δ_y, and δ_z represent the line displacement in the x, y, and z directions, respectively. θ_x, θ_y, and θ_z represent the angular displacement in the x, y, and z directions, respectively. The accurate stress results in finite element analysis can be obtained by applying boundary conditions more efficiently. There is only one longitudinal bulkhead in the cabin calculation model. Therefore, the strength of 8 working conditions is calculated according to relevant specifications. Conditions 1, 2, 3, and 6 are in navigation state. Conditions 4, 5, and 7 are in port state. Condition 8 is in ballast navigation state. The most dangerous working condition is the vertical state in working condition 2 after finite element static analysis. The stress results of various hull plate components are compiled under this working condition, as shown in Table 5.

Table 4: Boundary conditions

Constraint	Linear displacement			Angular displacement		
	δ_x	δ_y	δ_z	θ_x	θ_y	θ_z
End face A	/	Link	Link	Link	Link	/
End face B	/	Link	Link	Link	Link	/
Independent point A	Cons	Cons	/	BM	Cons	Cons
Independent point B	Cons	Cons	/	BM	Cons	Cons
Middle longitudinal bulkhead	Cons	/	/	/	Cons	Cons

Table 5: Maximum equivalent stress and maximum shear stress of components

Component	Bottom plate	Bilge plate	Side shell	Inner bottom plate	Inner bottom inclined plate	Inner shell plate	Strength deck	Bottom girder
Maximum shear stress (N/mm^2)	/	77.5	91.2	/	100	90.1	/	105
Maximum equivalent stress (N/mm^2)	193	151	179	140	175	174	204	198
Component	Centerline bulkhead	Transverse bulkhead	Non-watertight horizontal frame	Watertight horizontal frame	Platform plate	7670 horizontal truss	13250 horizontal truss	19200 horizontal truss
Maximum shear stress (N/mm^2)	128	47	113	47.2	/	87.8	69	102
Maximum equivalent stress (N/mm^2)	226	87	206	83.9	106	154	134	191

According to the relevant guidelines for direct calculation of the oil tanker in Table 5, the stress values of these components are within the specified allowable stress range. That is to say, these components can be optimized, providing possibilities for subsequent structural optimization. Due to the large thickness of structural plates and cross-sectional dimensions of bone materials in oil tankers, using these two indicators as design variables may increase the difficulty of optimization and affect the optimization. Sensitivity analysis of the cabin structure needs to be carried out by selecting ISIGHT software and conducting sensitivity analysis through parameter testing method before optimizing the design. The parameter testing is a sensitivity analysis method for studying independent design variables. The core principle of this method is finite difference, which means that a single design variable is subjected to small perturbations while keeping other design variables constant. The derivative of the objective or constraint function with respect to this design variable is calculated using the difference formula, which is the sensitivity value. The objective or constraint functions are the mass of the cabin structure, the maximum equivalent stress, and the maximum shear stress. The equivalent stress takes into account the Max Von Mises theory. According to the Max Von Mises theory, the failure of a material depends only on whether the equivalent stress exceeds the yield limit of the

material. The material failure situation can be determined by combining stress in different directions into an equivalent stress value. The optimization design variables selected for the study are the geometric parameters of the ship, and parameter sensitivity analysis is conducted. Variable parameters can be changed arbitrarily during the optimization process. Fixed parameters are constant and cannot be changed arbitrarily during the ship construction process. Therefore, physical parameters are generally not selected as design variables, but rather the geometric parameters of the ship are selected as optimization design variables. The variable of parameters represents the thickness of different sheets. The structural bone material size is set as a constant. Therefore, the variable for optimized design can be obtained, which includes 35 variables such as the thickness of the bottom outer plate, the thickness of the side outer plate, and the thickness of the inner bottom plate. The sensitivity of these variables to the mass of the cabin section is calculated. Based on the calculation results, the sensitivity values of all design variables are positive, indicating a positive correlation with the mass of the cabin section. The structural weight can be reduced by lowering the values of each design variable. Among these components, the sensitivity values corresponding to 8 design variables, such as the ship's bottom plate and side outer plate, are relatively high. Their proportion in the design variables is small, at 22%, and their contribution to the structural mass reaches 67%. Therefore, these sensitivity values can be considered as optimization design variables. On this basis, the maximum equivalent stress sensitivity and maximum shear stress sensitivity of the design variables are calculated. Based on these calculation results, the design variables with higher sensitivity are selected after comprehensive consideration. The remaining variables are filtered out. As a result, six optimization design variables, including the thickness of the bottom plate and the strong deck plate, can be obtained.

The BP neural network is used as a mapping model between structural plate thickness and response. This algorithm can only be constructed through sample data. The structure of the BP neural network is shown in Figure 5.

In Figure 5, the BP neural network consists of an input layer, a hidden layer, and an output layer. The neurons in the hidden layer use an S-shaped double tangent transfer function. The neurons in the output layer use a linear transfer function. The nodes in the input, hidden, and output layers are 6, 13, and 1, respectively. Therefore, the quality of sample data can be improved. The orthogonal design method is used to obtain sample data based on the BP neural network [21]. The selection of experimental factors is on the basis of the six optimization design variables obtained above, with a factor level of 5. The experimental orthogonal table is L25 (56). 25 and 6 represent the number of rows and columns in the orthogonal table. L represents the orthogonal table code. The experimental plan is determined and the thickness of each group of test plates is introduced into the model. The relevant results of the cabin section are obtained after the finite element calculation. The final sample data consists of 130 sets after comprehensive consideration. The training sample set consists of 105 sets of data. Partial sample data are shown in Figure 6.

In Figure 6, there are certain differences in the thickness of the component plates under different test times. Among the test times from 1 to 5, the thickness of the bottom plate is the same, all of which are 19mm.

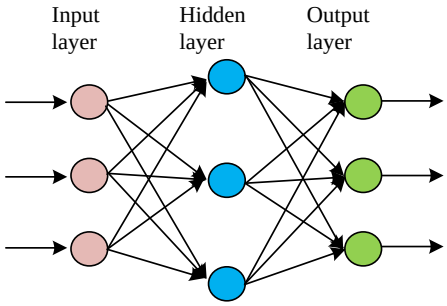

Figure 5: BP neural network structure diagram

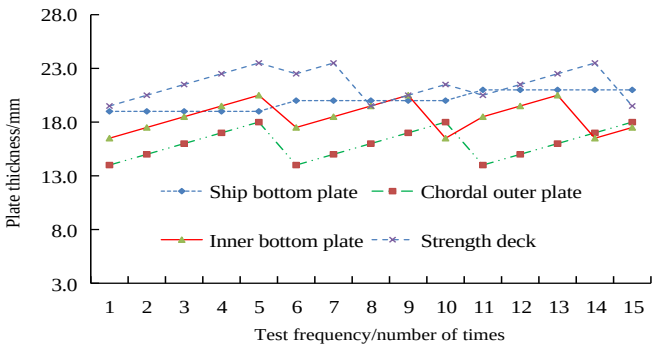

Figure 6: Partial sample data

3.2 Optimization design of cabin structure on the ground of SMPSO-BP neural network

An experiment is conducted on structural optimization design methods after obtaining the sample data. The BP neural network has a tendency to converge to local minimum. Therefore, this algorithm is improved by selecting the PSO algorithm. The PSO algorithm has strong global search ability and can compensate for the shortcomings of the BP neural network. Firstly, the study maps the weights and thresholds of the BP neural network to PSO algorithm particles. The mean square error function of the BP neural network is obtained through the PSO algorithm fitness function, and the specific mathematical expression is shown in equation (5).

$$f = \frac{1}{n}\sum_{j=1}^{n}\sum_{k=1}^{m}(y_{jk} - t_{jk})^2 \tag{5}$$

In equation (5), y_k means the actual output of the BP neural network. The expected output of the algorithm is set to t_k. Both k and j represent serial numbers. The number of training samples is set to n, and the number of output nodes of the BP neural network can be expressed as m'. The PSO-BP neural network is shown in Figure 7.

In Figure 7, first, the relevant parameters of the BP and PSO algorithms are initialized. The mathematical expression of the variable dimension D' is shown in equation (6).

$$D = inputnum \times hiddennum + hiddennum + hiddennum \times outputnum + outputnum \tag{6}$$

In equation (6), the number of input and output layer nodes is set to $inputnum$ and $outputnum$, respectively. $hiddennum$ means the number of hidden layer nodes. The individual extreme value $pbest$ and the global extreme value $gbest$ are initialized. The initial position of the particles is mapped to the initial weights and thresholds of the BP neural network. According to equation (5), the particle fitness is obtained, and the position of the particle with the lowest fitness is treated as $gbest$, with $pbest$ as the initial position of the particle. The particle position and velocity are updated. The specific update formula is shown in equation (7).

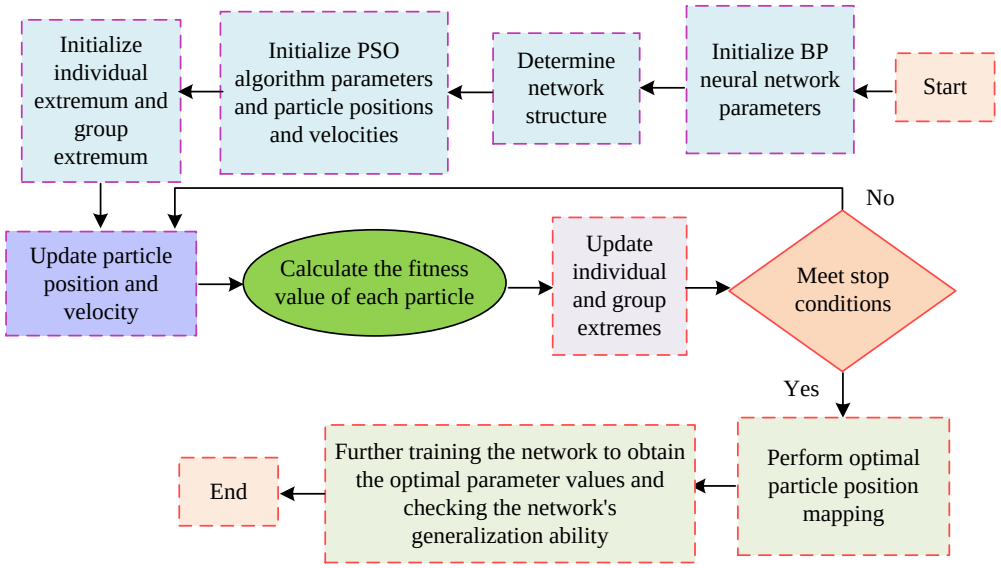

Figure 7: Related processes

$$\begin{cases} x_{id}(t+1) = x_{id}(t) + v_{id}(t+1) \\ v_{id}(t+1) = \omega(t)v_{id}(t) + \\ c_1 r_1(p_{id} - x_{id}(t)) + c_2 r_2(p_{gd} - x_{id}(t)) \end{cases} \tag{7}$$

In equation (7), $x_{id}(t)$ and $v_{id}(t)$ denote the current positions and velocities of the particles; $x_{id}(t+1)$ and $v_{id}(t+1)$ denote the updated positions and velocities of the particles. p_{id} denotes the individual optimum found by the particles. p_{gd} denotes the population global optimum. $\omega(t)$ denotes the inertia weights. c_1 and c_2 denote the learning factors. r_1 and r_2 denote the random numbers between [0,1]. The fitness values of particles are calculated. $pbest$ and $gbest$ are updated. $gbest$ and the current maximum iteration number are tested. If $gbest$ is greater than the target value or the iteration number is smaller than the maximum iteration, the particle position and velocity are re-updated. Subsequent steps are continued. On the contrary, the iteration is stopped. The particle position vector corresponding to $gbest$ is mapped to the initial weights and thresholds of the BP neural network. Although the PSO algorithm has a certain improvement effect on the BP neural network, the convergence effect of the BP neural network is not satisfactory and can only converge to the local optimal solution due to the previous

algorithm's inability to maintain population diversity. In this study, a staged mutation strategy is used to obtain the Staging Mutation Particle Swarm Optimization (SMPSO) algorithm and optimize the PSO algorithm. The process of SMPSO algorithm is shown in Figure 8.

In Figure 8, at the beginning stage of algorithm iteration, Multiple Interval Particle Swarm Optimization (MIPSO) is used to improve the way particles generate initial positions. Therefore, particles can be more evenly distributed in the search space. In the middle and later stages, the PSO algorithm is randomly perturbed *gbest* under the influence of chaotic algorithms, allowing the PSO algorithm to jump out of local minima. Overall, the process of the SMPSO-BP neural network is shown in Figure 9.

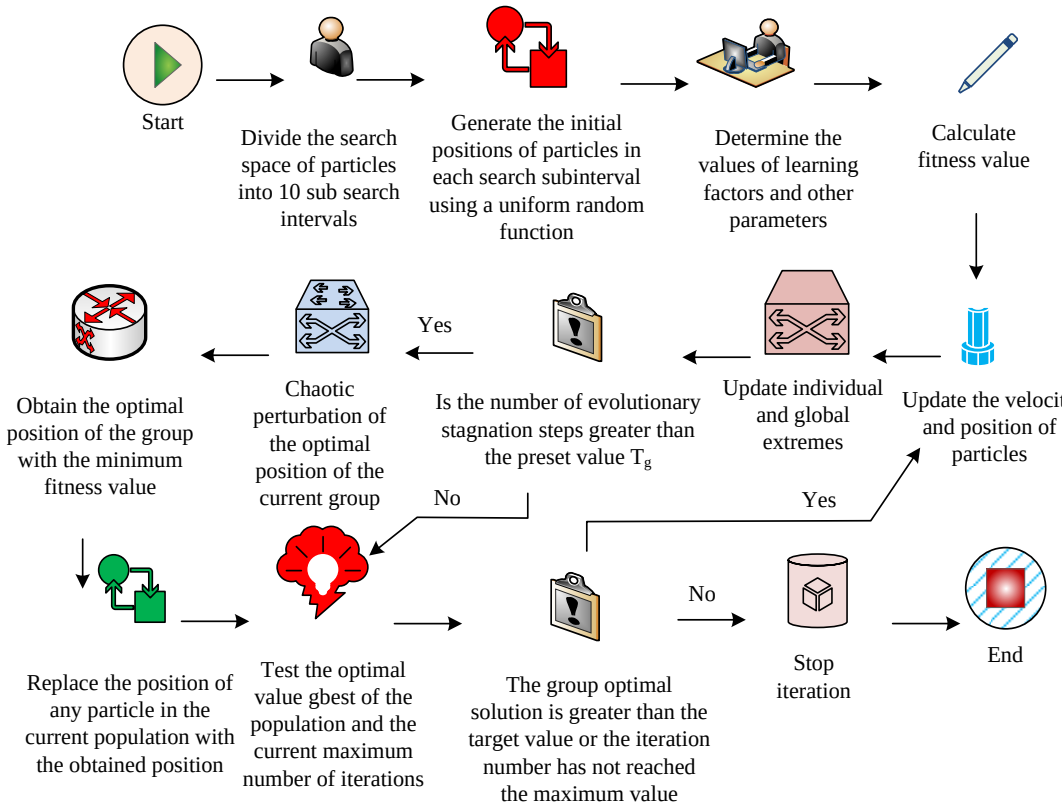

Figure 8: MIPSO algorithm flowchart

In Figure 9, the parameters of the BP neural network and PSO algorithm, such as *pbest* and *gbest*, are initialized. The initialization process is the same as in Figure 7. The particle velocity and position are updated. If the particle fitness value is smaller than the historical *pbest*, the current position *pbest* is adjusted. On the contrary, the current *gbest* is considered as the particle position. The number of evolutionary stagnation steps of *gbest* is judged and whether the number exceeds the preset T_g is analyzed. If the number exceeds T_g, the chaotic perturbation is applied to the current *gbest*, and the expression of *gbest* is shown in equation (8).

$$gbest = (p_{g1}, p_{g2}, \cdots, p_{gD}) \tag{8}$$

In equation (8), p represents the element in *gbest*. i represents the number. $gbest_i$ is mapped to the domain of the cubic chaotic system [-1,1]. The mapping result is treated as the initial value of the cubic chaotic equation z_i. The expression for z_i is shown in equation (9).

$$z_i = \left(gbest_i - a_i\right)/\left(b_i - a_i\right) \tag{9}$$

In equation (9), a_i represents the maximum $gbest_i$ in the i-th dimension. The minimum value in that dimension is set to b_i. A chaotic variable sequence z_i is obtained through $z_i^{(F)}(F = 1, 2\cdots)$, where F represents the variable. $z_i^{(F)}$ inverse is mapped to the original search space, resulting in $gbest_i^{(F)} = (p_{g1}^{(F)}, p_{g2}^{(F)}, \cdots, p_{gD}^{(F)})$. The fitness value of each $gbest_i^{(F)}$ is calculated to obtain the $gbest^*$ with the lowest fitness value, otherwise this step is skipped. The position of any particle in the current population is replaced with $gbest^*$ and the current maximum iteration and *gbest* are tested. The testing steps are the same as those in Figure 7. Simulation analysis is conducted on the SMPSO-BP neural network. The parameter settings are shown in Table 6.

In Table 6, the learning rate of the BP neural network is 0.1. The mathematical model for optimizing the cabin structure is shown in equation (10).

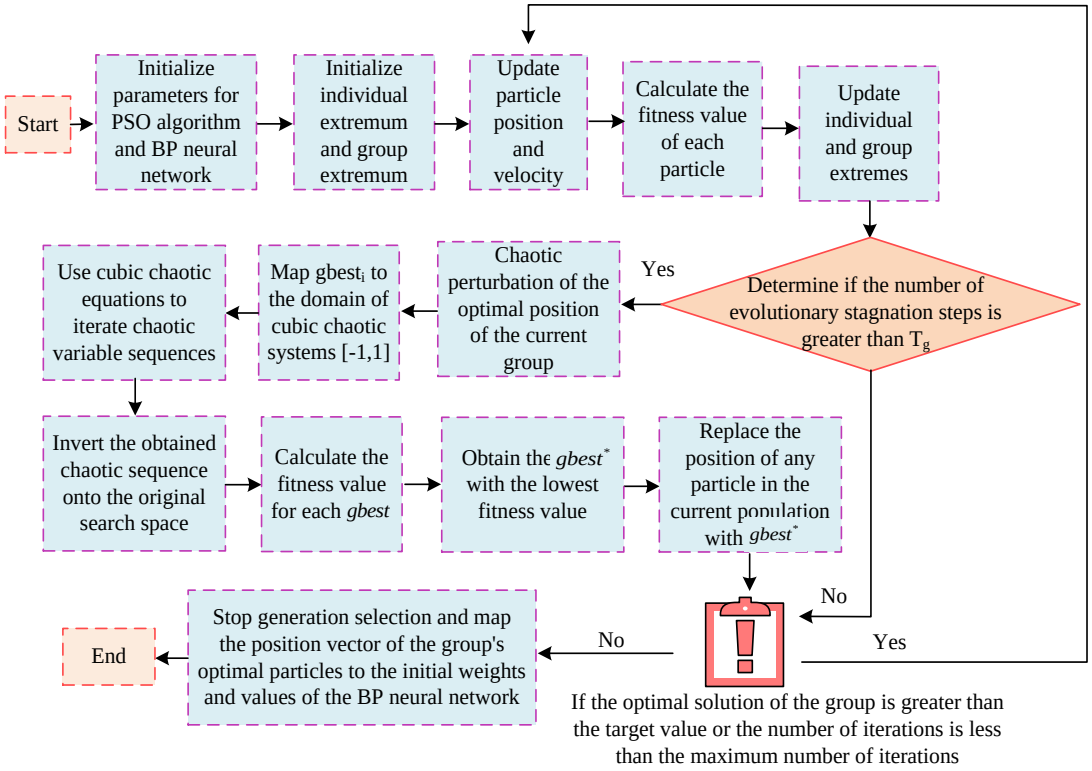

Figure 9: The process of the SMPSO-BP neural network

Table 6: Parameter settings

Algorithm	Parameter	Value
BP neural network	Training target error	0.00001
	Maximum number of iterations (times)	2000
	Learning rate	0.1
SMPSO algorithm	Population size	30
	Number of particles in each sub-interval (number)	3
	Learning factors	$c_1 = c_2 = 2$
	Maximum speed	0.5
	Maximum iteration (times)	5000
	Maximum number of iterations for cubic chaotic systems (times)	60
	T_g	5

$$\begin{cases} find & x_i \\ \min & F(X) \quad X \in R^n \\ s.t & G_j(X) \le 0, (j = 1, 2, \cdots, m) \\ & H_k(X) = 0, (k = 1, 2, \cdots, l) \end{cases} \tag{10}$$

In equation (10), x_i means the optimal solution of the design variable. The column vector composed of structural optimization design variables is represented as $X = [x_1, x_2, \cdots x_{n'}]^T$. n' represents the number of x. The objective function of structural optimization is set to $F(X)$. The inequality and equality constraint functions of structural optimization are set to $G_j(X) \le 0$ and $H_k(X) = 0$, respectively. The minimum thickness, maximum equivalent stress, and maximum shear stress of the selected components should be less than the corresponding allowable stress according to the requirements of the "Classification Code for Steel Seagoing Ships 2012" for large oil tanker components. The SMPSO-BP neural network is used to predict and output these stresses. The expression for $F(X)$ is shown in equation (11).

$$F(X) = \sum_{i=1}^{n'} \rho_i V_i = \sum_{i=1}^{n'} \rho_i S_i t_i \tag{11}$$

In equation (11), ρ represents the density of the component material. As the materials are all steel, the

density is taken as 7850kg/m3. V, S, and t represent the volume, area, and thickness of the component, respectively. The objective function is to minimize the weight of the oil tanker compartment. Matlab software is chosen. The cabin structure design is optimized through the constraint minimization function fmincon of the software. The optimization is constrained by the prediction results of the SMPSO-BP neural network. The fmincon function is nonlinearly constrained. The SMPSO-BP neural network converges continuously through iteration when the weight of the oil tanker compartment structure is the lightest.

4 Experimental results

Firstly, the MIPSO algorithm was validated using the collected real sample data. PSO-BP neural network was introduced for comparison. Secondly, the performance of the MSPSO-BP neural network was examined. Finally, the SMPSO-BP neural network was used to optimize the mathematical model for the optimization of the ship segment structure for calculation and analysis. Other algorithms were introduced for convergence performance comparison.

4.1 The Performance of MIPSO-BP neural network

The Matlab software was chosen to analyze the optimal fitness and error of the research method. Meanwhile, the convergence of the method was revealed. The training sample set had 105 sets of data. The testing sample set had 25 sets of data. The performance of the MIPSO-BP neural network was verified. The parameter settings are shown in Table 4. The PSO-BP neural network was used as the comparison algorithm. The initial position and velocity of particles in the PSO algorithm were taken as random numbers between [- l, 1]. The number of particles in each sub-interval of the MIPSO algorithm was 3, with a maximum particle velocity of 0.5. The maximum iteration for the cubic chaotic system was 60. Both neural networks were trained 10 times. The two neural networks were compared in terms of initial particle distribution, optimal solution of PSO algorithm, and network generalization ability. The initial particle distribution of the two algorithms was obtained in Figure 10.

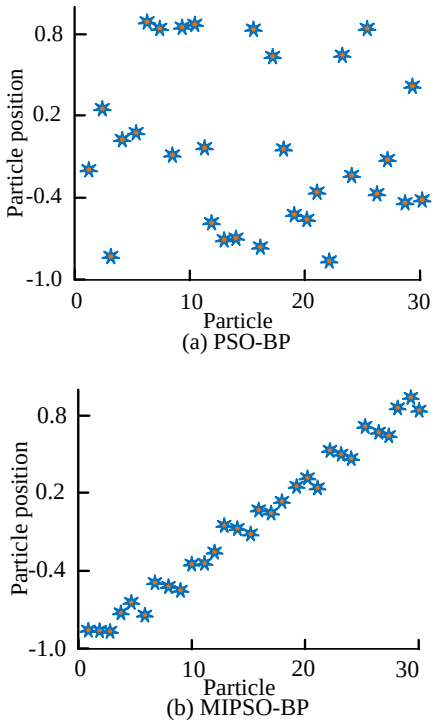

Figure 10: Initial distribution of particles

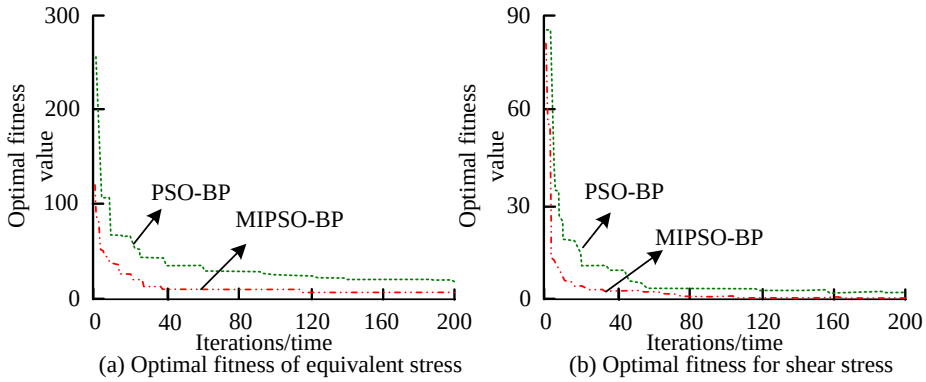

Figure 11: Initial distribution of particles

In Figure 10 (a), the initial particle position distribution randomly generated by the PSO-BP neural network was uneven, with 1 particle in the interval [0.2, 0.4], which was 5 fewer than the interval [0.8, 1.0], and 3 particles in the interval [-0.6, -0.8]. Compared to Figure 10 (a), the initial distribution of particles in Figure 10 (b) was relatively uniform. The algorithm pre-divided 10 sub-intervals, and the particle positions were randomly generated within the corresponding intervals, with 3 particles in each sub-interval. The optimal fitness values

for equivalent stress and shear stress of these two algorithms were analyzed in Figure 11.

In Figure 11 (a), the MIPSO-BP neural network had a faster convergence speed compared to the PSO-BP neural network. The MIPSO-BP neural network had an initial optimal fitness value of 121.4, which was 136.2 lower than the PSO-BP neural network's 257.6. The MIPSO-BP neural network began to converge at 115 iterations, while the PSO-BP neural network did not yet converge at 200 iterations. In Figure 11 (b), when the iteration number was 160, the optimal fitness value of the MIPSO-BP neural network for shear stress was 0, which was 3.7 times smaller than the PSO-BP neural network. Therefore, the MIPSO algorithm performed well and improved the performance of the BP neural network. The analysis of the SMPSO-BP neural network and the optimal solution of the PSO-BP neural network are shown in Figure 12.

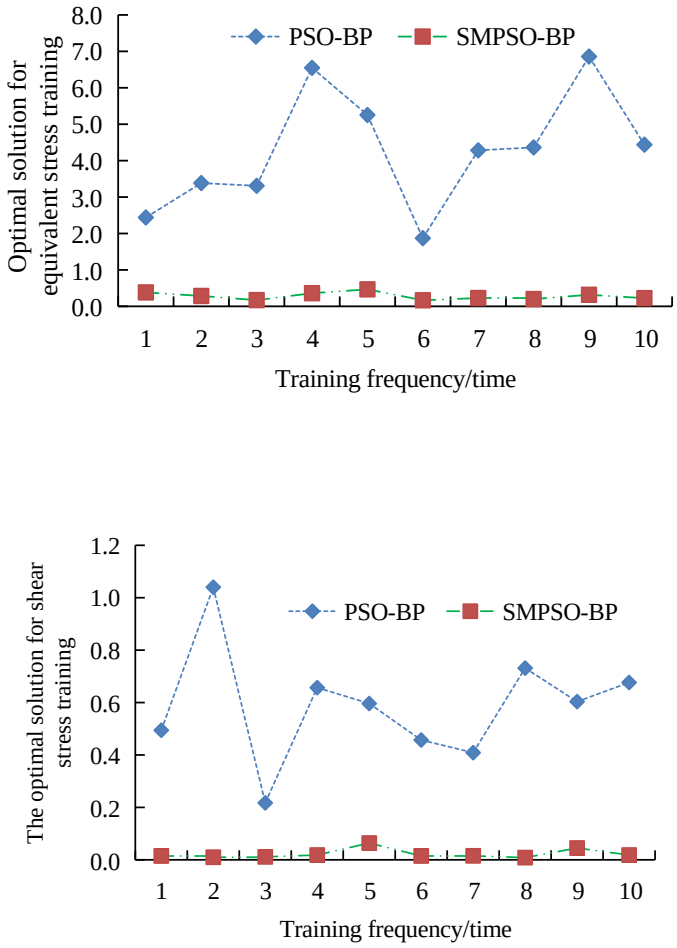

Figure 12: The optimal solution of the algorithm

In Figure 12 (a), the SMPSO-BP neural network had a smaller optimal solution for equivalent stress compared to the PSO-BP neural network. When the training frequency was 1, the optimal equivalent stress solution of the SMPSO-BP neural network was 0.3825, which was 2.0575 less than that of the PSO-BP neural network. When the training frequency was 5 times, the maximum equivalent stress optimal solution of the SMPSO-BP neural network was 0.4670, which was smaller than that of the PSO-BP neural network. In Figure 12 (b), the maximum and minimum values of the optimal shear stress solution for the SMPSO-BP neural network were 0.0640 and 0.0084, respectively, which were smaller than those of the PSO-BP neural network. A comparison of the diversity of the two algorithms is then shown in Figure 13.

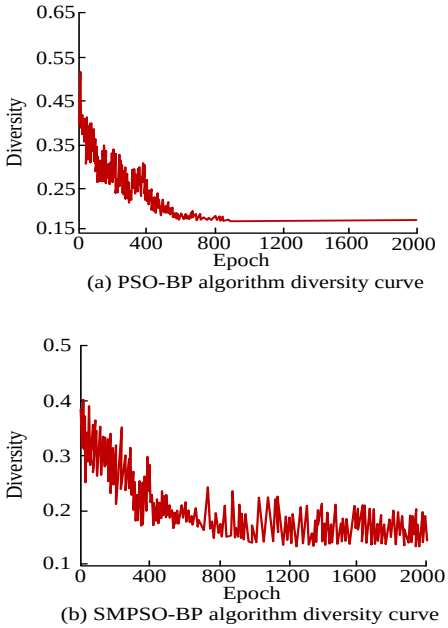

Figure 13: Comparison of algorithmic diversity

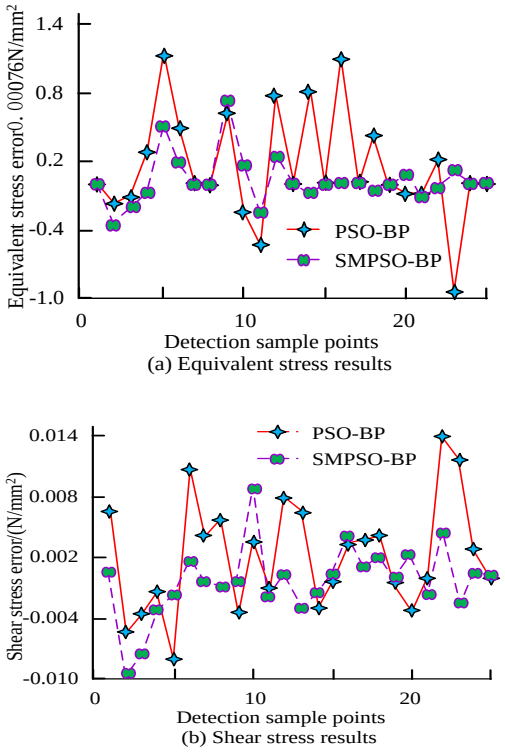

Figure 14: Detection error of two algorithms

Comparing the population location diversity of the two algorithms in Figure 7(a) and (b), both algorithms showed an overall oscillating downward trend in the early stage of iterative evolution. While in the late iteration, the diversity of the SMPSO-BP neural network oscillated above and below 0.16. The diversity of the PSO-BP neural network was stable and consistent. The ideal population diversity curve is often slowly decreasing and with large oscillations, showing superior ability to balance global and local search. Therefore, this can indicate that the population diversity of the proposed SMPSO-BP neural network is better. This may be due to the fact that the chaotic perturbation strategy maintains a continuous change in the population diversity of the algorithm. The detection errors of these two algorithms were analyzed in Figure 14.

In Figure 14 (a), the SMPSO-BP neural network had smaller line fluctuations and more stable prediction errors compared to the PSO-BP neural network. In sample point 5, the equivalent stress error of the SMPSO-BP neural network was 0.49N/mm^2, which was 0.64N/mm^2 less than the PSO-BP neural network. The equivalent stress error of the latter was 1.13N/mm^2. In Figure 14 (b), the SMPSO-BP neural network had a smoother line compared to the PSO-BP neural network. In sample point 10, the shear stress errors of the PSO-BP and SMPSO-BP neural networks were 0.0079N/mm^2 and 0.0003N/mm^2, respectively, with the former being 0.00076N/mm^2 larger than the latter. Therefore, the performance of the research method was better.

4.2 Analysis of optimization results for tank section structure of oil tankers

The SMPSO-BP neural network was applied to the structural optimization of oil tanker compartments, the fmincon function ran in Matlab software. The optimal plate thickness of the components was analyzed in Figure 15.

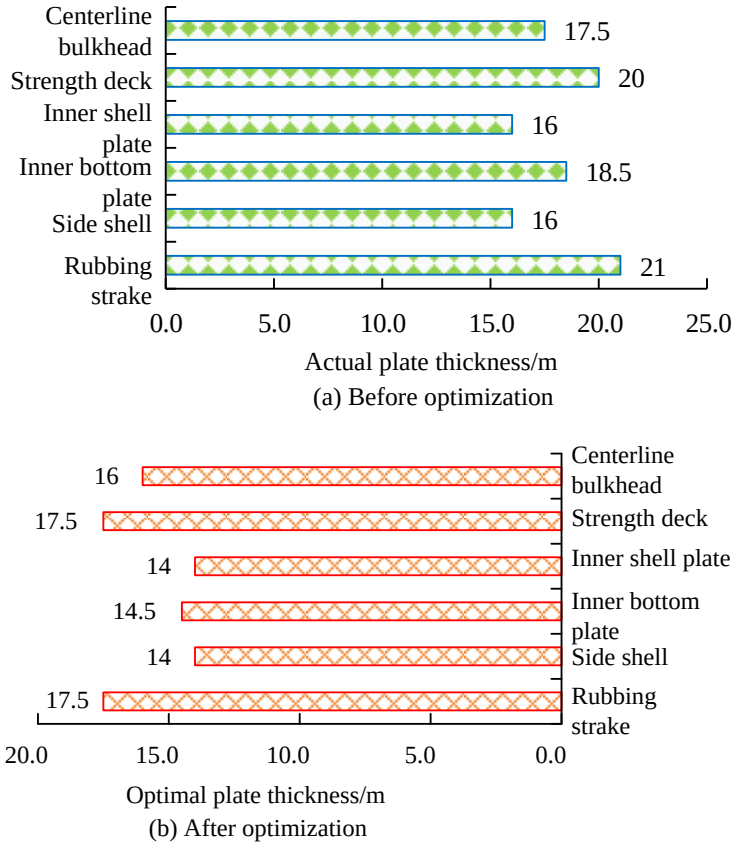

Figure 15: Actual plate thickness and optimal plate thickness

Figure 15 (a) shows the actual plate thickness of different components. The actual plate thickness of the bottom outer plate was 21.0m, which was 1.0m larger than the strong deck. The inner shell plate thickness was 16.0m. The thickness of the component plates in Figure 15 (b) decreased compared to Figure 15 (a). The optimal thickness of the bottom outer plate was 17.5m, which was 3.5m less than its actual thickness. The optimal thicknesses of the side outer plate and inner shell plate were both 14.0m. The relevant stress situation of some components after optimizing the middle section of the oil tanker is shown in Figure 16.

In the two sub-graphs of Figure 16, the equivalent stress and shear stress of the components increased after the optimization design. However, both were within the allowable values. In Figure 16 (a), for the equivalent stress of the ship's bottom plate, the pre-optimization value was 193N/mm^2, which was 23N/mm^2 smaller than the optimization value, and its allowable value was 305N/mm^2. The equivalent stresses before and after optimizing the inner bottom plate were 140N/mm^2 and 160N/mm^2, respectively. In Figure 16 (b), the shear stress of the inner bottom inclined plate before optimization was 100N/mm^2, which was 7N/mm^2 lower than the optimization value and 60N/mm^2 lower than the allowable value. The finite element analysis calibration showed that the stresses were improved and met the requirements. The above results implied that the optimized tanker section structure reduced the use of materials and improved the utilization of steel while maintaining or improving its load carrying capacity.

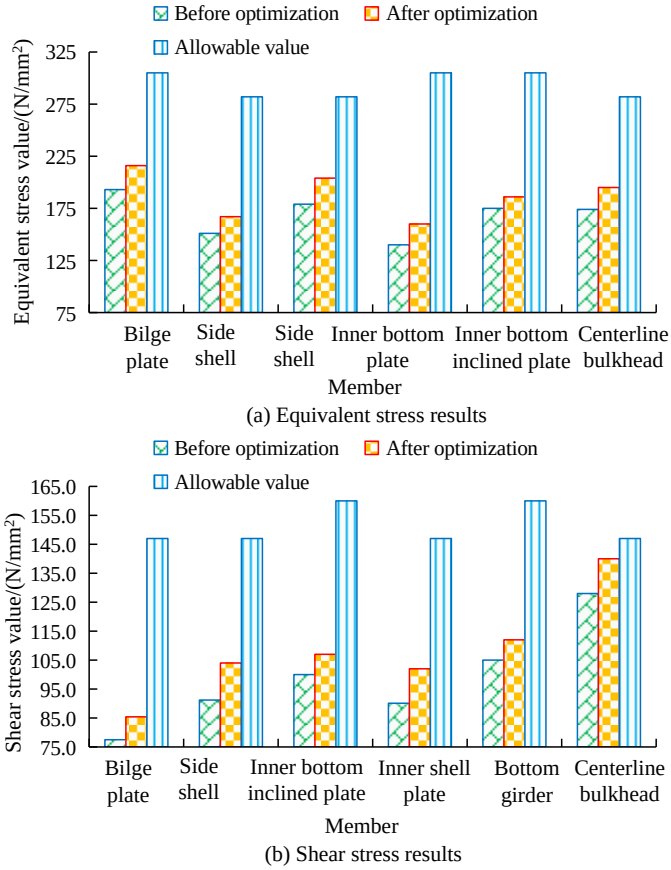

Figure 16: Actual plate thickness and optimal plate thickness

This is of great significance for reducing shipbuilding costs and improving economic efficiency. In addition, the optimized stress distribution was more reasonable, which was conducive to improving the durability and reliability of the structure, thus enhancing the integrity of the overall structure. The comparative methods include the improved Long Short-Term Memory (LSTM) [22] and the improved Wavelet Neural Network (WNN) [23] to analyze the weight of cabin segments under different iterations and different methods, as shown in Figure 17.

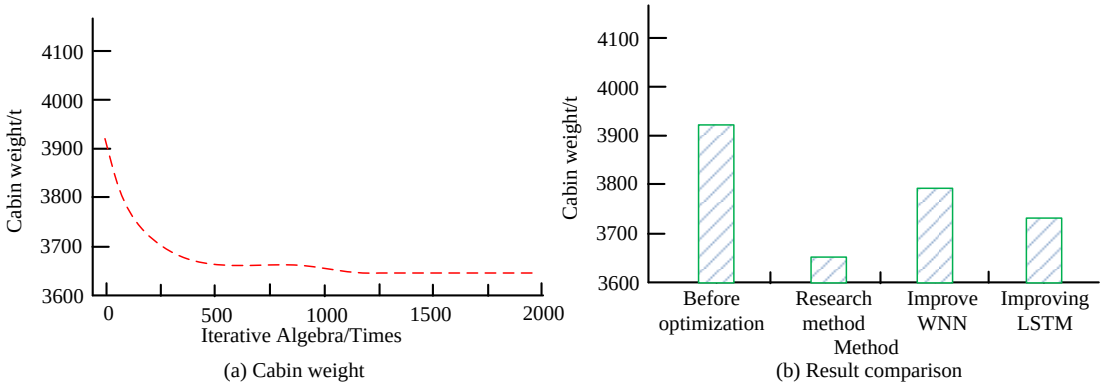

Figure 17: Section weight situation

In Figure 17 (a), the weight of the cabin segment processed by the research method varied under different iterations. When the iteration was 0, the weight of the cabin segment before optimization was 3912.45 tons. When the iteration was 1130, the algorithm began to converge, and the minimum weight of the cabin segment was 3648.49t. In Figure 17 (b), the cabin weight under the research method was the smallest compared to other methods, which was 78.04t smaller than the improved LSTM's 3726.53t. Therefore, the research method had

good performance and effectively reduced the steels used in the hull. Finally, the study further compares the convergence time and convergence performance of SMPSO-BP with MIPSO-BP, PSO-BP, LSTM, and WNN as shown in Table 7.

Table 7: Comparison of convergence performance of different methods

Method	Time (s)	Accuracy (%)
PSO-BP	4.23	82.03
MIPSO-BP	1.02	92.45
SMPSO-BP	0.95	97.87
LSTM	1.87	94.33
WNN	1.53	95.06

Comparison of Table 7 showed that the convergence time required for MIPSO-BP and SMPSO-BP was significantly lower than the other algorithms. The convergence time required for SMPSO-BP was only 0.95 s, with an accuracy of 97.87%. The accuracy of SMPSO-BP was increased by 19.31%, 3.75%, and 2.96% compared to PSO-BP, LSTM, and WNN, respectively. This indicated that the research algorithm greatly reduced the computational time overhead and improved the computational efficiency and algorithmic performance.

5 Discussion

The MIPSO-BP neural network had smaller errors compared to the PSO-BP neural network. In sample point 5, the equivalent stress error of the SMPSO-BP neural network was 0.49N/mm^2, which was 0.64N/mm^2 smaller than the PSO-BP neural network. The study utilized chaotic sequences to perturb the optimal position of the population, thereby avoiding the local minima. This can avoid the increased algorithm time caused by chaotic perturbations in each iteration, improve the performance of the PSO algorithm, and reduce the error of the MIPSO-BP neural network. In the research on optimal trajectory planning for robots, Du Y et al. also improved the performance of the PSO algorithm through hybrid motion, thereby shortening the running time of the robotic arm [24]. This is to some extent consistent with the strategy of studying and optimizing PSO algorithms. In the control of multi-system robots by Xu Z et al., the PSO algorithm was optimized by introducing hybrid motion, thereby improving the accuracy of the method [25]. There are similarities between the optimization method and the research method. In the parameter identification of Li M et al.'s photovoltaic model, a hybrid disturbance mechanism was added around the global optimal solution to achieve better identification results [26]. Therefore, the convergence speed of the PSO algorithm was improved. This optimization method is to some extent consistent with this study, that is, the optimization method studied is effective.

The proposed method not only synthesizes the self-learning ability of BP neural network and the global search ability of PSO algorithm. The generalization ability and prediction accuracy of the network are effectively improved by optimizing the weights and thresholds of the BP neural network through the improved PSO algorithm. In addition, the SMPSO-BP neural network can converge to the optimal solution more quickly and reduce the computation time when dealing with the ship structure optimization problem, which is of great significance for practical engineering applications. The study novelty lies in the successful application of the staged variation strategy to the PSO algorithm to optimize the BP neural network. In addition, this study provides a new method for the optimal design of ship compartment structures. This study has significant results in reducing material usage, lowering shipbuilding costs, and improving structural performance. These contributions not only promote the technological progress in the ship design, but also provide valuable references for other engineering fields.

In the future, the research will further optimize the algorithm to improve its application. First, the proposed method can be applied to different types of ships and more complex structural components to verify its versatility and adaptability. Second, more design parameters are considered in the optimization, such as the spacing and size of the transverse strong frame, to achieve a more comprehensive structural optimization. In addition, further research is conducted to improve the algorithmic computational efficiency and robustness, especially when dealing with large-scale and multi-objective optimization problems. Finally, the possibility of combining the proposed method with other optimization techniques or artificial intelligence methods is explored to further improve the optimization performance.

6 Conclusion

The finite element analysis of oil tanker compartments was studied to optimize the structure of oil tanker compartments. A 3D two-compartment model was constructed to analyze the stress results of various hull components under the most dangerous working conditions and to determine whether there is room for optimization in the oil tanker. On this basis, sensitivity analysis of cabin structure and sample acquisition was carried out. The performance of the PSO-BP neural network was improved by using a staged mutation strategy to optimize the PSO algorithm. A cabin structure

optimization model was constructed, and constraints were determined. Relevant predictions were made by improving the BP neural network. The results showed that the MIPSO-BP neural network had a more uniform initial particle distribution compared to the PSO-BP neural network. The algorithm pre-divided 10 sub-intervals, each randomly generating 3 particles. The PSO-BP neural network had 1 particle in the interval [0.2, 0.4], which was 5 fewer than the interval [0.8, 1.0]. The SMPSO-BP neural network had a smaller optimal solution for equivalent stress compared to the PSO-BP neural network. When the training frequency was 1, the optimal equivalent stress solution of the SMPSO-BP neural network was 0.3825, which was 2.0575 less than the PSO-BP neural network. The stress on the cabin components increased after structural optimization. For the equivalent stress of the ship's bottom plate, the value before optimization was 193N/mm^2, which was 23N/mm^2 lower than the optimization value. The weight of the cabin segment obtained by the research method was relatively small compared to other algorithms. The cabin weight obtained by the research method was 3648.49t, which was 78.04t smaller than the improved LSTM algorithm. Therefore, this study can effectively carry out the structural design of the cabin section. However, the research still needs further improvement, such as application verification in different types of ships and other complex structures. Future research also needs to consider the adaptability and robustness of the algorithm, further enhancing its universality and practicality. Meanwhile, the study only considers the thickness of the component plate as a variable in the optimization of the cabin structure and treats other parameters as known quantities. In the future, parameters such as the spacing of the horizontal strong FR can be added to the optimization of the cabin structure.

7 Nomenclature

All symbols and abbreviations:

Project	Meaning
BP	Back Propagation
PSO	Particle Swarm Optimization
SAH	A certain steel material
AH	A certain steel material
P_0	The reference water pressure
C_w	The wave coefficient
D	The mold depth
L	The standard ship length
d	The design structure draft
P	The pressure of liquid cargo in the tank
ρ_0	The density of liquid cargo in the tank
g	The gravitational acceleration
h	The vertical distance from the top of the cabin to the calculation point
M	The end face bending moment
M_w	The wave bending moment
M_s	The static water bending moment
M_r	The corrected bending moment
L_0	The total length of the cabin model
Q_m	The linear uniformly distributed pressure of the middle compartment model
Q_e	The linear uniformly distributed pressure of The two end compartments
δ_x	The line displacement in the x direction
x	The x direction
y	The y direction
z	The z direction
δ_y	The line displacement in the y direction
δ_z	The line displacement in the z direction
θ_x	The angular displacement in the x direction
θ_y	The angular displacement in the y direction
θ_z	The angular displacement in the z direction
ISIGHT	Analysis software

L	The orthogonal table code
y_k	The actual output of the BP neural network
t_k	The expected output of the algorithm
k	Serial number
j	Serial number
n	The number of training samples
$inputnum$	The number of input
$outputnum$	The number of output layer nodes
$hiddennum$	The number of hidden layer nodes
$pbest$	The individual extreme value
$gbest$	The global extreme value
SMPSO	Staging Mutation Particle Swarm Optimization
MIPSO	Multiple Interval Particle Swarm Optimization
T_g	The preset value
p	The element in $gbest$
i	The number
z_i	The cubic chaotic equation
a_i	The maximum value of $gbest_i$ in the i -th dimension
F	The variable
$z_i^{(F)}$	Chaotic variable sequence
$gbest^*$	Global extremum with minimum fitness value
c_1	The learning factor
c_2	The learning factor
x_i	The optimal solution of the design variable
n'	the number of x
$F(X)$	The objective function of structural optimization
$G_j(X) \le 0$	The inequality constraint function
$H_k(X) = 0$	The equality constraint function
ρ	The density of the component material
V	The volume of the component
S	The area of the component
t	The thickness of the component
LSTM	Long Short-Term Memory
WNN	Wavelet Neural Network
PID	Proportional-Integral-Derivative

8 Fundings

The research is supported by Education Reform Project of Jiangsu Shipping Vocational and Technical College (No. HYJY/2022C06); Research Project on Vocational Education Teaching Reform in Jiangsu Province (No. ZYB653).

References

[1] C. Pany, S. Parthan, and M. Mukhopadhyay, "Wave propagation in orthogonally supported periodic curved panels," Journal of Engineering Mechanics, vol. 129, no. 3, pp. 342-349, 2003. https://doi.org/10.1061/(ASCE)0733-9399(2003)129:3(342)

[2] A. De, J. Wang, and M. K. Tiwari, "Hybridizing basic variable neighborhood search with particle swarm optimization for solving sustainable ship routing and bunker management problem," IEEE Transactions on Intelligent Transportation Systems, vol. 21, no.3, pp. 986-997, 2019. https://doi.org/10.1109/TITS.2019.2900490

[3] C. Song, and W. Cui, "Review of underwater ship hull cleaning technologies," Journal of Marine Science and Application, vol. 19, no. 3, pp. 415-429, 2020. https://doi.org/10.1007/s11804-020-00157-z

[4] C. Pany, S. Parthan, and M. Mukhopadhyay, "Free vibration analysis of an orthogonally supported multi-span curved panel," Journal of Sound and Vibration, vol. 241, no. 2, pp. 315-318, 2001. https://doi.org/10.1006/jsvi.2000.3240

[5] C. Pany, and G. Li, "Application of periodic structure theory with finite element approach," Frontiers in

Mechanical Engineering, vol. 9, pp. 1192657, 2023. https://doi.org/10.3389/fmech.2023.1192657

[6] X. Ren, Z. Huang, Y. Jiang, Z. H. Chen, X. F. Cao, T. Zhao, and Y. Li, "The scaling laws of cabin structures subjected to internal blast loading: Experimental and numerical studies," Defence Technology, vol. 18, no. 5, pp. 811-822, 2022. https://doi.org/10.1016/j.dt.2021.04.001

[7] C. Pany, S. Parthan, and S. Mukherjee, "Vibration analysis of multi-supported curved panel using the periodic structure approach," International Journal of Mechanical Sciences, vol. 44, no. 2, pp. 269-285, 2002. https://doi.org/10.1016/S0020-7403(01)00099-6

[8] R. R. Asaad, and R. I. Ali, "Back propagation neural network (BPNN) and sigmoid activation function in multi-layer networks," Academic Journal of Nawroz University, vol. 8, no. 4, pp. 216-221, 2019. https://doi.org/10.25007/ajnu.v8n4a464

[9] F. Lian, J. Jin, and Z. Yang, "Optimal container ship size: a global cost minimization approach," Maritime Policy & Management, vol. 46, no. 7, pp. 802-817, 2019. https://doi.org/10.1080/03088839.2019.1630760

[10] R. Dai, Y. Liu, Y. Cheng, J. Liu, and P. Zhang, "Topology and opening size optimization design of solid floors in an outer tank of the pressure hull," Chinese Journal of Ship Research, vol. 14, no. 6, pp. 139-146, 2019. https://doi.org/10.19693/j.issn.1673-3185.01460

[11] N. M. Ameen, and A. T. Humod, "Robust nonlinear PD controller for ship steering autopilot system based on particle swarm optimization technique," IAES International Journal of Artificial Intelligence, vol. 9, no. 4, pp. 662-669, 2020. https://doi.org/10.11591/ijai.v9.i4.pp662-669

[12] S. Guo, X. Zhang, Y. Zheng, and Y. Du, "An autonomous path planning model for unmanned ships based on deep reinforcement learning," Sensors, vol. 20, no. 2, pp. 1-34, 2020. https://doi.org/10.3390/s20020426

[13] H. Zakerdoost, and H. Ghassemi, "Hydrodynamic decomposition-based optimization of ship's hull–propeller system under multiple operating conditions," Journal of Ship Production and Design, vol. 39, no. 01, pp. 32-42, 2023. https://doi.org/10.5957/JSPD.10180038

[14] Z. Zhang, J. Yin, N. Wang, and Z. G. Hui, "Vessel traffic flow analysis and prediction by an improved PSO-BP mechanism based on AIS data," Evolving Systems, vol. 10, no. 3, pp. 397-407, 2019. https://doi.org/10.1007/s12530-018-9243-y

[15] Y. Liu, J. Kang, Y. Bai, and C. Guo, "Research on the health status evaluation method of rolling bearing based on EMD-GA-BP," Quality and Reliability Engineering International, 2023. https://doi.org/10.1002/qre.3350

[16] J. Lu, Q. You, M. Zhang, and X. Jiang, "Ship boiler steam pressure control system based on BP-PID control," EPH-International Journal of Applied Science, vol. 5, no. 1, pp. 13-17, 2019. https://doi.org/10.53555/eijas.v5i1.88

[17] D. Zhang, "Fault diagnosis of ship power equipment based on adaptive neural network," International Journal of Emerging Electric Power Systems, vol. 23, no. 6, pp. 779-791, 2022. https://doi.org/10.1515/ijeeps-2022-0103

[18] C. Pany, and S. Parthan, "Axial wave propagation in infinitely long periodic curved panels," Journal of Vibration and Acoustics, vol. 125, no. 1, pp. 24-30, 2003. https://doi.org/10.1115/1.1526510

[19] C. Pany, "An insight on the estimation of wave propagation constants in an orthogonal grid of a simple line-supported periodic plate using a finite element mathematical model," Frontiers in Mechanical Engineering, vol. 8, pp. 926559, 2022. https://doi.org/10.3389/fmech.2022.926559

[20] C. Pany, and S. Parthan, "Flutter analysis of periodically supported curved panels," Journal of sound and vibration, vol. 267, no. 2, pp. 267-278, 2003. https://doi.org/10.1016/S0022-460X(02)01493-1

[21] J. Purohit, and R. Dave, "Leveraging deep learning techniques to obtain efficacious segmentation results," Archives of Advanced Engineering Science, vol. 1, no. 1, pp. 11-26, 2023. https://doi.org/10.47852/bonviewAAES32021220

[22] P. Nagabushanam, S. Thomas George, and S. Radha, "EEG signal classification using LSTM and improved neural network algorithms," Soft Computing, vol. 24, no. 13, pp. 9981-10003, 2020. https://doi.org/10.1007/s00500-019-04515-0

[23] Q. Chen, Y. Song, and J. Zhao, "Short-term traffic flow prediction based on improved wavelet neural network," Neural Computing and Applications, vol. 33, no. 14, pp. 8181-8190, 2021. https://doi.org/10.1007/s00521-020-04932-5

[24] Y. Du, and Y. Chen, "Time optimal trajectory planning algorithm for robotic manipulator based on locally chaotic particle swarm optimization," Chinese Journal of Electronics, vol. 31, no. 5, pp. 906-914, 2022. https://doi.org/10.1049/cje.2021.00.373

[25] Z. Xu, L. Du, H. Wang, and Z. Deng, "Particle swarm optimization-based algorithm of a symplectic method for robotic dynamics and control," Applied Mathematics and Mechanics, vol. 40, no. 1, pp. 111-126, 2019. https://doi.org/10.1007/s10483-019-2412-6

[26] M. Li, C. Li, Z. Huang, J. Huang, G. Wang, and P. X. Liu, "Spiral-based chaotic chicken swarm optimization algorithm for parameters identification of photovoltaic models," Soft Computing, vol. 25, no. 20, pp. 12875-12898, 2021. https://doi.org/10.1007/s00500-021-06010-x